LC-DET-2000-046
Updated Version 07/08/2002

Møller Scattering Polarimetry for High Energy e^+e^- Linear Colliders

GIDEON ALEXANDER[1,2]
Institut für Physik
Humboldt-Universität zu Berlin, Germany
11015 Berlin, Germany

and

IULIANA COHEN
School of Physics and Astronomy
Raymond and Beverly Sackler Faculty of Exact Sciences
Tel-Aviv University, Tel-Aviv 69978, Israel

Abstract

The general features of the Møller scattering and its use as an electron polarimeter are described and studied in view of the planned future high energy e^+e^- linear colliders. In particular the study concentrates on the TESLA collider which is planned to operate with longitudinal polarised beams at a centre of mass energy of the order of 0.5 TeV with a luminosity of 3.4×10^{34} cm^{-2}sec^{-1}.

PACS 29.25.Pj; 29.27.Hj; 34.80Nz;
Keywords: Electron beam polarisation, Linear collider, Møller polarimeter

[1]Permanent address: Physics department, Tel-Aviv University, Tel-Aviv, Israel.
[2]Corresponding author, Tel: +972-3-6408240, Fax: +972-3-6407932,
e-mail: alex@lep1.tau.ac.il, (G. Alexander).

Contents

1 Introduction

It is for some time that the high energy physics community is of the opinion that in the near future there will be a need for the facilities of a high energy linear e^+e^- colliders. Currently under discussion are several linear colliders which should reach centre of mass (CM) energies up to 3 TeV, the features of which, can be found e.g. in Ref. [1]. Among them the TESLA collider, aimed to run at 0.5 TeV, is already in a rather advanced study and planning stage [2]. It has been further pointed out that the option of longitudinal polarised electron beams in such high energy colliders, like TESLA, will enrich significantly the physics capabilities of the device [3]. The use of polarised beams requires however a continuous monitoring and sufficient accurate measurement of the beam polarisation during the entire collider operation.

In addition to the widely used $\gamma e \to \gamma e$ Compton scattering polarimeter, the $e^-e^- \to e^-e^-$ Møller scattering process has also been utilised to evaluate the polarisation level of the electron beams. Unlike the Compton polarimeter the operation of a Møller polarimeter may need dedicated accelerator runs but its relatively simple construction and operation and high counting rates makes it nevertheless a rather attractive device. Even though the Møller polarimeter is primarily used for the measurements of the electron beam polarisation it can also be applied, almost without any modification, to the measurement of the positron beam polarisation by replacing the Møller process with the Bhabha elastic scattering [4].

Several colliders have in fact already used Møller polarimeters to monitor their polarised electron beams. The Stanford Linear Collider (SLC) has primarily used a precise Compton polarimeter to monitor the beam and measure the electron beam polarisation [5, 6]. In addition it has also engaged two single-arm Møller polarimeter for beam polarisation diagnosis. Many fixed target experiments, e.g. those described in references [7–10], were running with polarised beams monitored by Møller polarimeters. Finally the Møller like scattering, $\mu e \to \mu e$, was used in the SMC experiment at CERN [11] to measure the polarisation of the muon beam. The Møller measurement may also be applied after the colliding beams interaction point (IP). For this purpose, the Møller polarimeters are more suited for the NLC, JLC or CLIC linear colliders, than for TESLA, because of their non-zero angle crossing, which avoids the need to bend after the IP the beams trajectories into the dumping area.

In this paper we describe the outcome of a detailed study which explored the feasibility and usefulness of the Møller scattering process to serve as a method for the longitudinal polarisation measurement. To this end we chose the features of the planned TESLA to represent a typical electron-positron collider at high energies. In Sections 2 and 3 we describe in some details the various properties of the Møller scattering, with and without polarised beams, and also review some of the technical characteristics of the Møller polarimeters used in recent high energy experiments emphasising the specific TESLA needs. The expected event rates and the effects of the energy deposition in the target by the electron beam are dealt with in Section 4. In Section 5 we describe the proposed method for the beam polarisation measurement and evaluate its expected performance. Finally, in Section 6, the effects of the background sources on the polarimeter performance are evaluated.

2 The Møller scattering

2.1 The basic formulae for $e^-e^- \rightarrow e^-e^-$ scattering

The Møller $e^-e^- \rightarrow e^-e^-$ differential cross section, at tree level, is getting contributions from the s and t photon exchange channels. In the CM system it is given by:

$$\frac{d\sigma}{d\Omega} = \frac{\alpha^2}{s}\frac{(3+\cos^2\theta)^2}{\sin^4\theta} \times F_{pol} \tag{1}$$

for high $E^2_{CM} = s$ values where the electron mass squared m_e^2 can be neglected. The factor F_{pol} is the function describing the dependence of the differential elastic cross section on the polarisation of the electron which is given by :

$$F_{pol} = 1 - P_L^B P_L^T A_L(\theta) - P_t^B P_t^T A_t(\theta)\cos(2\phi - \phi_B - \phi_T) \ . \tag{2}$$

Here:
α = the fine structure constant at low energies which is equal to 1/137;
θ = the CM system polar scattering angle;
ϕ = the CM azimuthal angle of the scattered electron;
P_L^B and P_L^T = longitudinal polarisation of the beam and target;

P_t^B and P_t^T = transverse polarisation of the beam and target;
ϕ_B and ϕ_T = the azimuthal angles of the beam and target transverse polarisation vectors.

The longitudinal and transverse asymmetry functions, $A_L(\theta)$ and $A_t(\theta)$, are defined as:

$$A_L(\theta) \;=\; \frac{(7+\cos^2\theta)\sin^2\theta}{(3+\cos^2\theta)^2} \qquad \text{and} \qquad \mathrm{A_t}(\theta) \;=\; \frac{\sin^4\theta}{(3+\cos^2\theta)^2}\,. \tag{3}$$

To note is that both $A_L(\theta)$ and $A_t(\theta)$ are small in the forward direction so that the asymmetries are small in the region where the t-channel diagram dominates.

In order to determine the beam polarisation, the rate of the electrons scattered in a given solid angle $d\Omega$ is measured in one orientation of the beam and target polarisation vectors $(\vec{P}^{\,B}, \vec{P}^{\,T})$ and then with the beam polarisation vector inverted i.e., $(-\vec{P}^{\,B}, \vec{P}^{\,T})$. Here the polarisation vectors are defined as $\vec{P}^{\,B} \equiv [P_L^B, P_t^B]$ for the beam and $\vec{P}^{\,T} \equiv [P_L^T, P_t^T]$ for the target. The longitudinal component, P_L, is in the z-direction and P_t, the transverse component, is perpendicular to that direction. Thus the two rates which one measures are:

$$R(s, \vec{P}^{\,B}, \vec{P}^{\,T}) \qquad \text{and} \qquad R(s, -\vec{P}^{\,B}, \vec{P}^{\,T})\,,$$

normalised to the same integrated luminosity. From these rates one constructs the asymmetry A_R which is equal to:

$$\begin{aligned} A_R \;&=\; \frac{R(s, \vec{P}^{\,B}, \vec{P}^{\,T}) - R(s, -\vec{P}^{\,B}, \vec{P}^{\,T})}{R(s, \vec{P}^{\,B}, \vec{P}^{\,T}) + R(s, -\vec{P}^{\,B}, \vec{P}^{\,T})} \\ &=\; -P_L^B P_L^T A_L(\theta) - P_t^B P_t^T A_t(\theta)\cos(2\phi - \phi_B - \phi_T). \end{aligned} \tag{4}$$

Finally the beam polarisation is extracted from the measured values of A_R, the known target polarisation and the unpolarised asymmetry functions given in Eq. 3.

The expressions given in Eqs. 1 and 4 are derived for the lowest order diagrams for the $e^-e^- \to e^-e^-$ process. The contributions of higher diagrams, up to order 4 in the fine structure constant α, were in the past investigated in [12] and more recently in [13]. The QED corrections to the Møller asymmetry can be evaluated through the BMOLLR code developed by S. Jadach and B. Ward [14]. This is an $\mathcal{O}(\alpha)$ exponentiated Monte Carlo (MC) generator for $e^-e^- \to e^-e^- + n\gamma$ for any n value.

2.2 Application to $e^+e^- \to e^+e^-$ scattering

The polarisation of the collider positron beam can also be measured by its elastic scattering, that is Bhabha scattering, on electrons in a polarised target.

The pure QED differential Bhabha cross section of polarised beam and target is expressed in the CM system by:

$$\frac{d\sigma}{d\Omega} = \frac{\alpha^2}{4s}\frac{(3+\cos^2\theta)^2}{(1-\cos\theta)^2} \times F_{pol} \,, \tag{5}$$

where F_{pol} is again given by Eq. 2 when $s \gg m_e^2$. Therefore in this case $A_L(\theta)$ and $A_t(\theta)$ are identical for the Møller and Bhabha processes, independent of the energy and symmetric around $\theta = 90^\text{o}$ in the CM system. Thus the polarisation level of the e^+ beam can also be estimated via the measurement of the asymmetry A_R previously defined in Eq. 4 for the Møller scattering.

The difference in the polarisation measurement between the Møller and Bhabha scattering lies however in their absolute cross section value and in their dependence on the polar angle θ . For the case of target electron in rest and $E_B = 250$ GeV, these differences are illustrated in Fig. 1. As expected, the Møller scattering is symmetric around $\cos\theta = 0$ whereas the Bhabha scattering is peaked in the forward direction. Furthermore, the Møller scattering cross section is higher than that of the Bhabha cross section and in particular at $\cos\theta = 0$, where the A_R asymmetry is maximal, the ratio of the two processes is equal to four.

In the following we address our study specifically to the Møller scattering process which in fact is also valid for the Bhabha scattering bearing in mind however that its event rate is smaller by a factor four and its background may be different.

2.3 Some general features

Some obvious features of the Møller scattering can be deduced from Eq. 1.

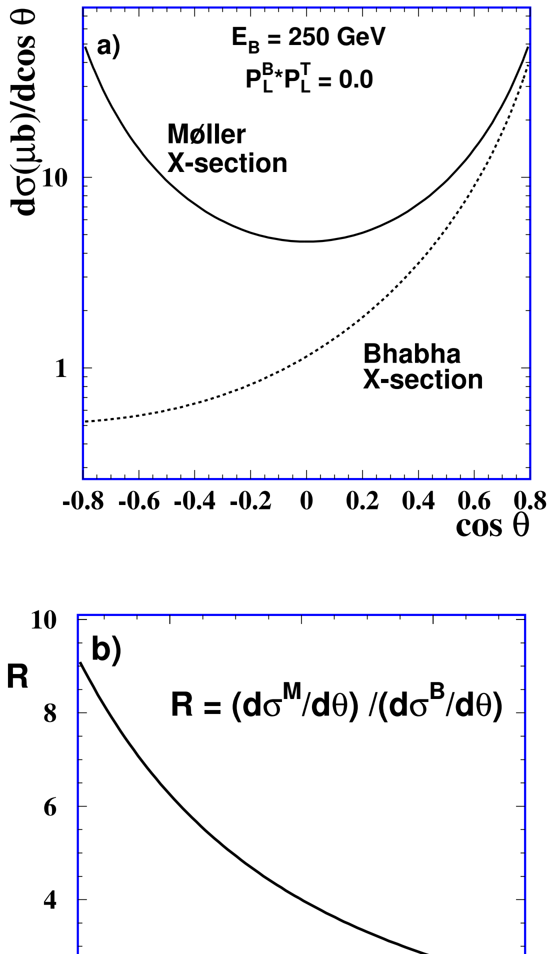

Figure 1: a) The Møller and Bhabha differential cross section, σ^M and σ^B, for $E_B = 250$ GeV and a target electron at rest, b) their ratio as a function of $\cos\theta$.

a) The cross section is seen to diverge at $\cos\theta = \pm 1$. This is due to the fact that the electron mass was neglected. In a rigorous treatment, where m_e is not neglected, the Møller scattering formula remains finite even at $\cos\theta = \pm 1$.
b) The cross section magnitude decreases as s increases, similar to the one photon annihilation process in e^+e^- annihilation.
c) Only if the beam and the target are simultaneously transverse and/or longitudinal polarised a change in the Møller scattering will be observed.
d) In the absence of transverse polarisation the cross section is independent of the azimuthal angle ϕ. This independence can also be achieved by integrating over the whole azimuthal angle ϕ provided of course that the experimental setup is ϕ independent.
e) The asymmetry functions reach their maximum at a CM scattering angle of $90^{\rm o}$ and approach zero in the forward and backward directions.

2.4 Differential cross sections and asymmetries

The cross sections and asymmetries were studied for a set of E_B values and several beam-target polarisation configurations where we set everywhere $\phi_B + \phi_T$ to zero, without a loss in generality. In order to illustrate the effects of the beam and target polarisations we assume for the target a polarisation of 90% realising that in practice an iron target has a maximum polarisation of 8%. The beam polarisation was taken to be 90%. In Fig. 2 we show, after integrating over the whole azimuthal angle ϕ, a typical CM polar angular distribution of the Møller scattering of a beam with the nominal energy of 250 GeV, scattered by a stationary electron target, without and with longitudinal polarisation characterised by their $P_L^B P_L^T$ values. For beam electrons of $E_B = 250$ GeV scattered over a stationary electron, we show in Fig. 3 a two dimensional plot of the Møller differential cross section $d^2\sigma/(d\cos\theta d\phi)$ having both a longitudinal and a transverse polarisation. In Fig. 4 we show the total Møller cross section integrated over ϕ from $0^{\rm o}$ to $360^{\rm o}$ and over the polar angle region $|\cos\theta| < 0.9$ for unpolarised and polarised beam and target. Finally we show in Fig. 5(left) the Møller scattering asymmetry, A_R, as a function of $\cos\theta$ and ϕ for a longitudinal and transverse polarisation values of $P_L^B P_L^T = 0.81$ and $P_t^B P_t^T = 0.81$. In the same figure we also show the asymmetry A_R dependence on $\cos\theta$ after integrating over the ϕ angle.

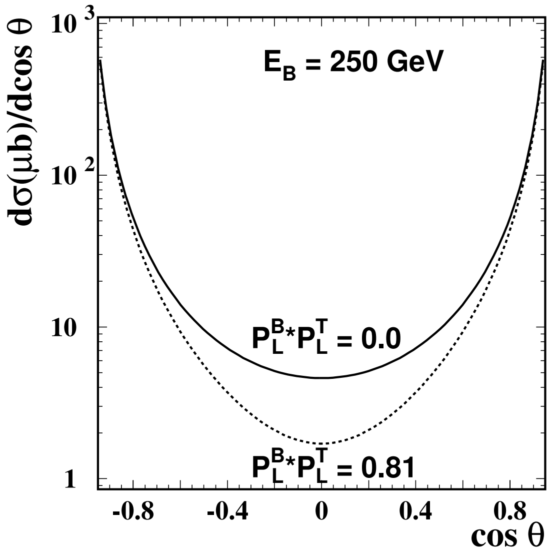

Figure 2: Møller differential cross section, $d\sigma/d\cos\theta$, as a function of $\cos\theta$ in the range of $|\cos\theta| < 0.9$ for $E_B = 250$ GeV without and with longitudinal polarisations.

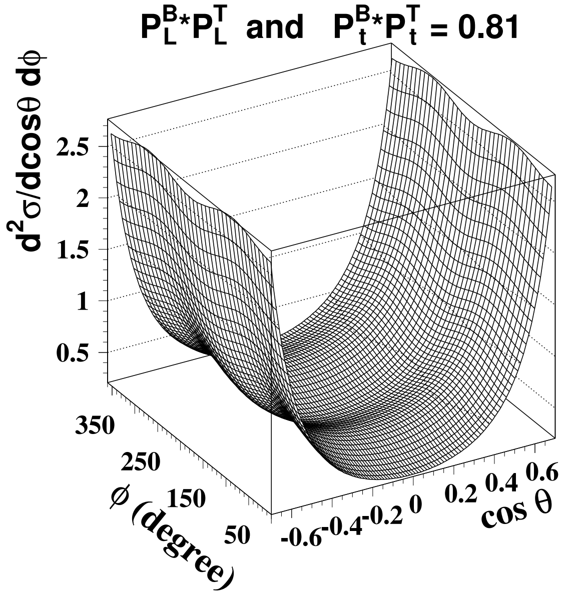

Figure 3: A two-dimensional plot of the Møller scattering $d^2\sigma/(d\cos\theta d\phi)$ in μb, for $E_B = 250$ GeV, is shown for the set of longitudinal and transverse polarisations values indicated in the figure.

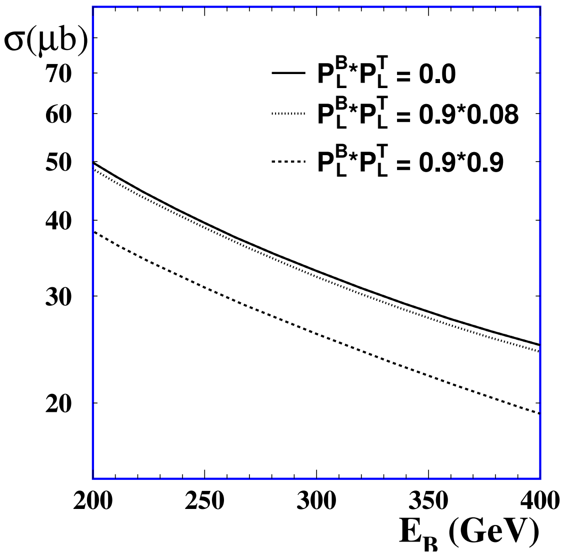

Figure 4: The total Møller scattering cross section, integrated over the range $0^o < \phi < 360^o$ and $|\cos\theta| < 0.9$, as a function of the beam energy without and with longitudinal polarisation. The target electron is taken to be at rest.

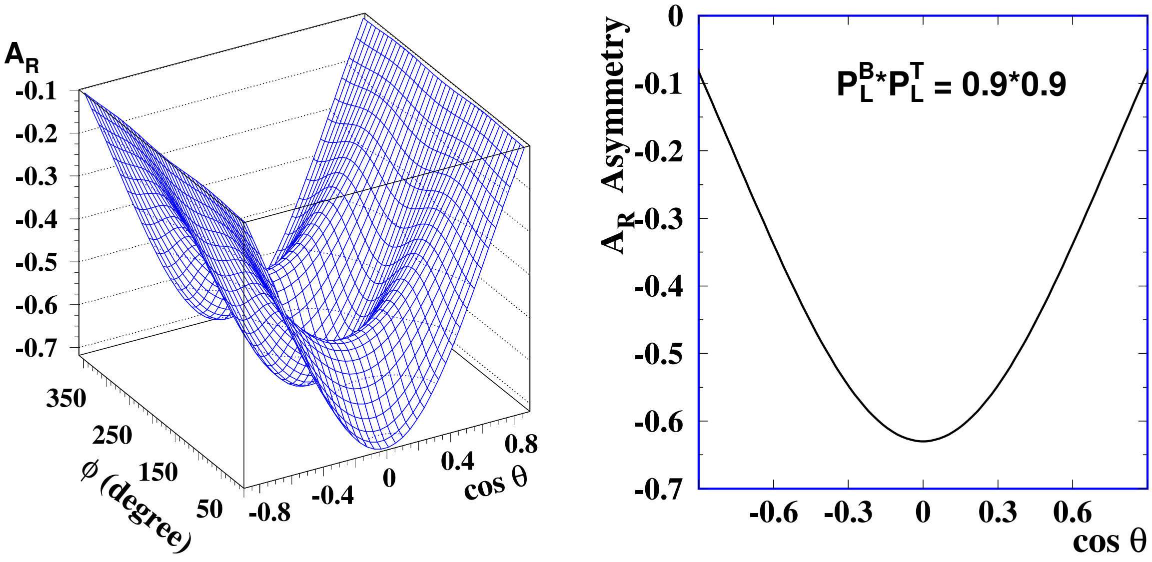

Figure 5: The Møller scattering asymmetry. Left, a 2-dimensional plot of A_R as a function of $\cos\theta$ and the azimuthal angle ϕ for $P_L^B P_L^T = 0.81$ and $P_t^B P_t^T = 0.81$. Right, A_R as a function of $\cos\theta$, integrated over $0^o < \phi < 360^o$ for $P_L^B P_L^T = 0.81$.

3 Møller scattering in the laboratory system

In the collision of two electrons the total centre of mass energy squared, s, may be written in the Lorentz invariant form, and thus valid in any reference system, as:

$$s = 2m_e^2 + 2E_B E_T(1 - \beta_B \beta_T \cos\theta_{1,2}) \ , \tag{6}$$

where E_B and E_T are the beam and target electron energies, $\theta_{1,2}$ is the angle between the incident particle's momenta and $\beta_{B,T} = p_{B,T}/E_{B,T}$ are the velocities of beam and target electrons.

At TESLA, where the beam energy is planned to reach a few hundreds GeV, one has $\beta_B = p_{_B}/E_{_B} \simeq 1$ so that one can neglect m_e^2 and Eq. 6 reduces to:

$$s = 2E_B E_T(1 - \beta_T \cos\theta_{1,2}) \ . \tag{7}$$

3.1 Target electrons at rest

In the approximation that the target electron is in the laboratory system a free particle at rest ($\beta_T = 0$), the square of the centre of mass energy is given by the expression:

$$s = 2E_B m_e = 2p_{_B} m_e \ , \tag{8}$$

where $p_{_B}$ is the beam momentum value. The laboratory momentum of the scattered electron , p_{lab}, is given by :

$$p_{lab} = \gamma_{_{\rm CM}} \sqrt{(E^* + p^* \beta_{_{\rm CM}} \cos\theta)^2 - \frac{m_e^2}{\gamma_{_{\rm CM}}^2}} \ , \tag{9}$$

where p^*, E^* are the momentum and energy of the incident electron in the CM system and $\gamma_{_{\rm CM}} = 1/\sqrt{1-\beta_{_{\rm CM}}^2}$. The relation between the laboratory scattering angle θ_{lab} and the CM scattering angle θ is given by:

$$\tan\theta_{lab} = \frac{1}{\gamma_{_{\rm CM}}} \times \frac{\sin\theta}{\beta_{_{\rm CM}}/\beta^* + cos\theta} \ , \tag{10}$$

where $\beta_{_{\rm CM}}$ is the velocity of the centre of mass system and β^* is the velocity of the electron in the CM system. For elastic scattering of a beam electron of E_B= 250 GeV on an electron at rest one has $m_e/E_{_B} = 2 \times 10^{-6} << 1$ so that Eqs. 9

and 10 can be reduced to a simpler form.

In the CM system of the Møller scattering the momentum and energy of the incident electron are expressed by:

$$p^* = \sqrt{\frac{m_e(E_B - m_e)}{2}} \quad \text{and} \quad E^* = \sqrt{\frac{m_e(E_B + m_e)}{2}} \; . \tag{11}$$

From Eqs. 8, 9, 10 and 11 follows that

$$p_{lab} = \frac{p_{_B}}{\sqrt{s}} \times \frac{\sqrt{s}}{2}(1+\cos\theta) = \frac{p_{_B}}{2}(1+\cos\theta) \; , \tag{12}$$

so that the laboratory momentum of the scattered electron does not depend on the CM total energy, but only on the beam energy and the CM scattering angle. From Eq. 10 one obtains, in a few simple steps, the expression:

$$\tan^2\theta_{lab} = \frac{2m_e}{E_B + m_e} \times \frac{1-\cos\theta}{1+\cos\theta} \; , \tag{13}$$

which in the small angle approximation can be written as

$$\theta^2_{lab} = 2m_e\left(\frac{1}{p_{lab}} - \frac{1}{p_{_B}}\right) \; . \tag{14}$$

The single-arm Møller polarimetry is based on Eq. 14 which provides the identification of the elastic e^-e^- scattering through the relation, in the laboratory system, between θ_{lab} and p_{lab}. In Fig. 6 we show the relation between the centre of mass polar angle θ and the angle of scattered electron θ_{lab}, for three different E_B values.

The analysing power of the Møller polarimeter is proportional to the product of the unpolarised cross section and the square of the asymmetry [5]. For longitudinal polarisation measurements, the analysing power is maximum at $\theta = 90^{\circ}$. In Fig. 6 the region of $\pm 10^{\circ}$ around this optimal θ value is magnified. For $\cos\theta = 0$ one has for any E_B the following Møller scattering relevant quantities:

$$A_L = \tfrac{7}{9}; \qquad A_t = \tfrac{1}{9} \quad \text{and} \quad A_R = -P_L^B P_L^T \times \tfrac{7}{9},$$

so that for $E_B = 250$ GeV one has:

$d\sigma/d\cos\theta|_{\cos\theta=0} = 4.55(1 - 7/9 \times P_L^B P_L^T)$ μbarn ;

$p_{lab} = 125$ GeV ;

$\theta_{lab} = 2$ mrad .

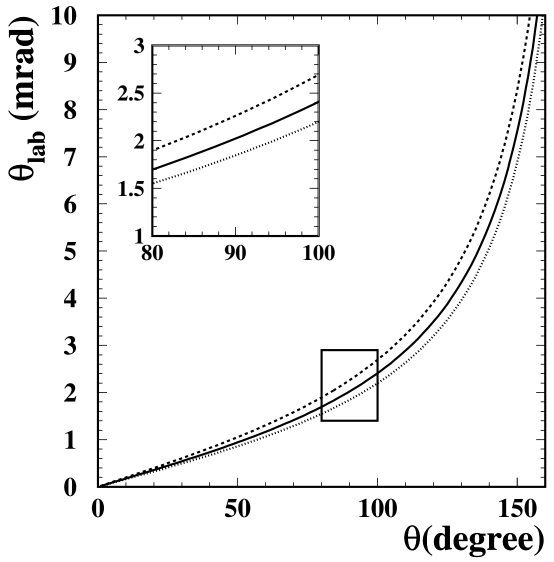

Figure 6: The Møller scattering angle, θ_{lab}, as a function of θ, the CM angle. The target electron is at rest. The solid line is drawn for $E_B = 250$ GeV , the dashed one corresponds to $E_B = 200$ GeV and the dotted one is for $E_B = 300$ GeV. The insert magnifies the region where $|A_R|$ is at or near its maximum.

3.2 Target electrons with non-zero momentum

The detailed kinematics of the scattering of an energetic electron from a bound state electron moving with momentum p_T (Fermi momentum) is discussed in [15]. This Fermi momentum can change the CM energy of the scattering process even when E_B remains the same. The ratio between the scattering CM energy, s' when the Fermi motion is taken into account to the CM energy, s, when the target electron is stationary is given, to a leading order, by:

$$\frac{s'}{s} = \left(1 - \frac{\vec{p}_T \cdot \vec{n}}{m_e}\right) \ , \tag{15}$$

where $\vec{p}_T$ is the momentum of the target particle and $\vec{n} = \vec{p}_B/p_B$ is the unit vector pointing in the direction of the beam particle momentum. The presence of non-zero momentum target electron does not modify Eq. 12 but Eq. 14 is changed producing the Levchuk effect namely, the line image in $\theta_{lab} - 1/p_{lab}$ space is broader.

Taking into account the corrected CM energy given by Eq. 15, one has to modify

Eq. 14 to read:

$$\theta_{lab}^2 = 2m_e \left(\frac{1}{p_{lab}} - \frac{1}{p_{_B}} \right) \left(1 \pm \frac{p_{_T}}{m_e} \right) \ . \tag{16}$$

The laboratory scattering angle is smeared by the square root of the target momentum dependent factor $1 \pm p_{_T}/m_e$, the same factor which modifies the CM energy.

In the experiments which operated during the last decade the targets used for the Møller polarimeters have been Fe alloy or pure Fe foils [6, 8, 9]. In these kind of materials the K- and L-shell electrons are unpolarised (with mean momentum of 90 keV and 30 keV) and the polarised ones reside in the M- and N-shells (with 10 keV and 2 keV average momenta). Only two electrons in the M-shell carry the Fe magnetisation, out of a total of 26, yielding a maximum target polarisation of 8%.

For the polarised target electrons the smearing factor is small but for unpolarised electrons from K-shell it can achieve values around 20%. In Fig. 7 we show the dependence of the scattering angle, θ_{lab}, on the CM angle θ for the case of target electrons at rest (solid line) and for moving target electrons from the M and K shells (dashed and dotted lines).

In Fig. 8 we plot the momentum of elastic scattered Møller electrons as a function of θ, the centre of mass polar angle, for three E_B values. As mentioned earlier, the momentum does not depend on s, the total CM energy squared (see Eq. 12), therefore it is not modified even when the Fermi motion of the target electrons are accounted for. This means that the lines shown in Fig. 8 are not affected by the motion of the target electrons and have not to be split for M and K atomic shells as is the case in Fig. 7.

For $E_B = 250$ GeV the factor $1/s$, which enters in Eq. 1, changes by about 18% when the target electron mean momentum increases from 0 to 90 keV.
The effect on the asymmetry however is smaller, namely $10 - 15\%$ and can be estimated by using a proper simulation of the elastic Møller signal (see e.g. reference [6]). Finally the measured polarisation value is shifted by about 10% pending on the material of the target, the resolution and acceptance of the polarimeter and the analysis procedure.

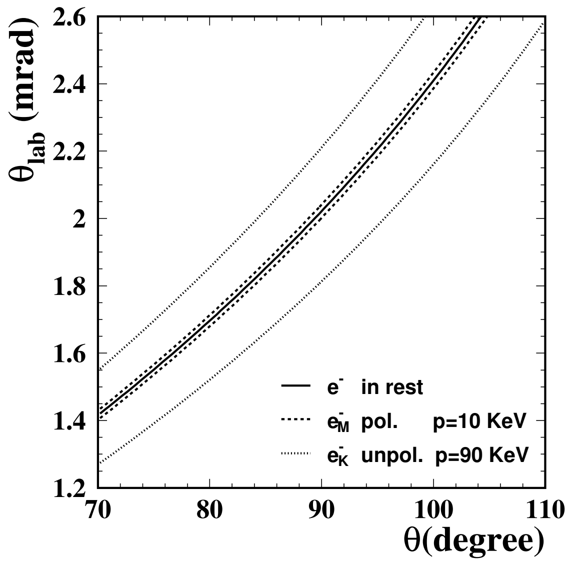

Figure 7: The Møller scattering angle, θ_{lab}, as a function of θ, the CM angle, for $E_B = 250$ GeV. The solid line is for target electrons at rest The dashed and dotted pair of lines correspond to the upper and lower limits of θ_{lab} for electrons from M and K atomic shells having the momentum of 10 and 90 keV respectively.

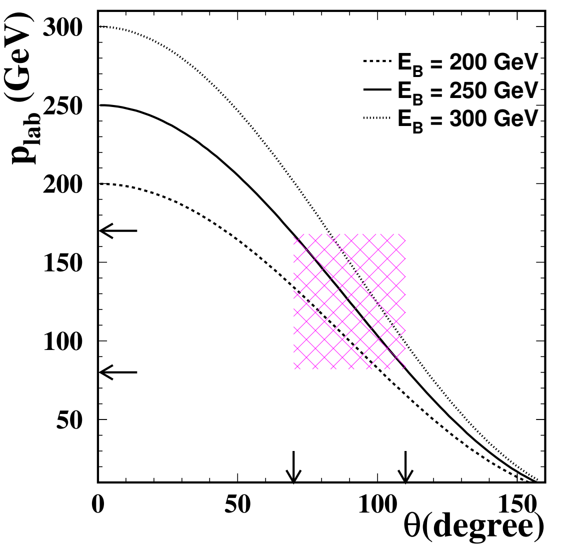

Figure 8: The Møller scattered electron momentum p_{lab}, as a function of θ, the CM scattering angle, for various beam energy values. The optimal working region is shown by the hatched area.

The correction needed to account for this shift depends on the details of polarimeter construction, the beam parameters and the analysis technique as is discussed e.g. in [6]. At SLC the effect was found to be large due to the low emittance of the beam and the fine resolution of the detector. The solution to this problem, already adopted by the E143 at SLC and the JLAB [7, 8] experiments, is given by adopting the coincidence measurement method in a double-arm polarimeter setup. These polarimeters have larger acceptance and poorer resolution so that the Levchuk effect was shown to be very small.

A recent study [16] on the performance of the double-arm polarimeter, has discovered a new effect arising from the Fermi motion of the atomic electrons in the target. Namely, that there exists a dependence of the measured Møller asymmetry on the relative position of the detectors in the double-arm operation mode. Here it should be point out that the technical design of a Møller polarimeter and its performance simulation can only be taken after the final design of the collider is available.

4 Beam - Target related features

A typical setup for Møller polarimeter can be found e.g. in Ref. [7]. The final design and exact position of the Møller polarimeter however does depend on the choice taken between a single or a double-arm device and on the detailed knowledge on the beam transport of the collider and background conditions. In these two possibilities the common elements of a Møller polarimeter are:

• A magnetised target made usually of a Fe or Fe-alloy foil or, if technologically feasible, a new type of target (see e.g. Ref. [17]);
• A set of magnets to steer the scattered electrons;
• A collimator to define the accepted scattering range in the azimuthal angle ϕ and the ($\theta_{lab}^{min} - \theta_{lab}^{max}$) polar angle interval, for the elastic scattered electrons. This is followed by a dipole magnet that selects electron momenta in the desired range of acceptance;
• Finally the scattered electrons are detected and registered by a pixel detector such as the hybrid silicon pixel sensors proposed in [18]. For special low luminosity

runs, aimed at checking the polarimeter performance, it may be advantageous to add behind the pixel detector an electromagnetic calorimeter to enable the simultaneous measurement of the position and energy of the scattered electrons.

4.1 Expected luminosity

The current design of the TESLA beam consists of the set of parameters given in Ref. [19] and listed here in Table 1. This information is here used to evaluate *the effective luminosity*[3], the expected rate of Møller scattering events and its heating effect on the target due to the energy deposited by the electron beam. To this end we consider the following target and electron beam features:

- For the target we choose a pure iron foil having an electron density of:

  $$\rho_e^{target} = N_A \cdot \rho \cdot \frac{\bar{Z}}{\bar{A}}, \tag{17}$$

  where N_A is the Avogadro number, ρ is the density of the material and $\bar{Z}, \bar{A}$ are the mean atomic number and atomic mass of the iron foil. Taking the density of this material to be $\rho = 7.87$ g/cm^3 and $\bar{Z}/\bar{A} = 466$ kg^{-1}, one obtains:

  $$\rho_e^{target} = 2.21 \cdot 10^{24} \text{electrons/cm}^3. \tag{18}$$

- For the planned beam current of $I_{beam} = 45$ μA, the number of electrons which hit the target in a time interval of one second is:

  $$N_e^{beam} = \frac{I_{beam}}{q_e} = 2.82 \cdot 10^{14} \ \text{ electrons/sec} . \tag{19}$$

4.2 Expected counting rates

The counting rate, defined as the number of Møller scattering events/sec, is given by:

$$\text{Rate} = d \times \rho_e^{target} \times N_e^{beam} \times \sigma_{mol} = \mathcal{L} \times \sigma_{mol}, \tag{20}$$

where $\mathcal{L}$ is the so called effective luminosity. The Møller scattering cross section, σ_{mol}, is the result of the integration of Eq. 1 over the whole azimuthal angle

[3] In the present context of fixed target scattering *the effective luminosity* is defined as the luminosity of the collider beam and the target electrons (see Eq. 20).

range and over a chosen CM polar angle θ domain of $|\cos\theta| < 0.34$, that is:

$$\sigma_{mol} = \int_0^{2\pi} d\phi \int_{-0.34}^{0.34} \frac{d\sigma}{d\cos\theta}(1 - P_L^B P_L^T A_L(\theta))\ d\cos\theta\ , \tag{21}$$

where

$$\frac{d\sigma}{dcos\theta} = \frac{\alpha^2}{2E_B m_e}\frac{(3+\cos^2\theta)^2}{\sin^4\theta}\ .$$

Using the relevant values obtained in subsection 4.1, we evaluate for a high beam polarisation of 80% and a Fe target polarisation of 8%, so that $P_L^B P_L^T = 0.8 \times 0.08$, the cross section and effective luminosity to be:

$$\sigma_{mol} = 3.3 \cdot 10^{-30}\ \text{cm}^2 \quad \text{and} \quad \mathcal{L} = 6.2 \cdot 10^{35}\ \text{cm}^{-2}\text{sec}^{-1}.$$

From Eq. 20 the expected rate of Møller events is then:

$$\text{Rate}\ =\ 20.6 \cdot 10^5\ \ \text{events/sec}\ .$$

One should point out that the values given here are summed over the whole ϕ angle range from 0 to 2π. In practice, the polarimeter acceptance covers only a small part of this range, denoted here by $\Delta\phi$. Therefore the last quoted rate has to be scaled down by the factor $\Delta\phi/2\pi$. For a polarimeter acceptance of $\Delta\phi = 2\pi/9$ rad and $\Delta\theta = 40^{\text{o}}$ the expected rate is

$$\text{Rate}\ =\ 2.28 \cdot 10^5\ \ \text{events/sec} = 228\ \text{kHz}\ ,$$

which is well within the range of the current capabilities of the data acquisition systems used for Møller polarimeters.

4.3 Target for precise Møller polarimetry

The target frequently used in Møller polarimeters consisted of thin foils of ferromagnetic alloy with the composition 49% Fe(Z=26, A=57.9), 49% Co(Z=27, A=58.9) and 2% Vanadium(Z=23, A=50.9) known under the name of Vanadium-Permendur alloy. It is magnetised *in-plane* using a pair of Helmholtz coils producing a small magnetic field of 0.01 T. The foils are usually mounted at an angle of $\sim 20^{\text{o}}$ with respect to the beam so that the target frame will not interfere with the beam trajectory[4]. The disadvantages of a target with *in-plane* magnetisation are: a poor knowledge of the target polarisation i.e. having an uncertainty of $\sim 1.5\% - 3.0\%$ as reported in Refs. [6, 7, 9, 10]; the demagnetisation due to the target heating is undetected and the target polarisation forms a non-zero angle with the beam direction.

In order to achieve a 1% precision measurements of the beam polarisation these limitations have to be overcome given their massive contributions to the systematic error. A novel approach adopted for the target construction has been recently developed and put to use [8, 20]. This target is made out of a thin *pure iron* foils polarised *out-of-plane* in saturation with a 4 T magnetic field parallel to the electron beam. The online measurement of the relative foil polarisation during the polarimeter operation is carried out with a laser beam making use of the polar Kerr effect [20].

This new target design allows to reach an accuracy of 0.5% on the target polarisation and thus meets the precision beam polarisation measurements requested e.g. by TESLA. This high precision was already obtained in an experiment which operated with an electron beam of few μA operating in the energy range of 1 to 6 GeV at the JLAB (see Ref. [8]).

4.4 The target temperature rise

Here we address the question of the target heating due to the energy deposited by the impinging beam and its possible effect on the polarimeter performance. To this end we consider a pure Fe foil target with a thickness of $d = 10$ μm and an area of about 30 cm^2 so that the target material seen by the beam is $\widetilde{\rho} = d \times \rho = 7.87 \cdot 10^{-3}$ g/cm^2. The target, which is cooled down to about 110 K, is polarised in saturation *out-of-plane*, so that when it is placed perpendicular to the beam direction the projected longitudinal polarisation of the target electrons is at its maximum.

[4] If the target is polarised *in plane* it has to be oriented at an angle $\psi \neq 0$ relative to the beam with the result that the relevant longitudinal polarisation of the target electrons is reduced to $P_L^T = P^T \cdot \cos\psi$ and its effective thickness is increased to $d_{eff} = d/\sin\psi$.

4.4.1 Local heating per bunch

The TESLA beam design envisages a pulse cycle of 5 Hz. The duration of each pulse is ~ 1 msec followed by a pause of ~ 199 msec. Each pulse contains 2820 bunches of 1 psec length each and repeated every 337 nsec.

The ionisation energy loss in the target of one beam electron with an energy of 250 GeV, is $dE_{ion}/dx = 2.5 \cdot 10^6$ eV/g/cm^2 (see e.g. Ref [21]). The energy, E, deposited in the target by one bunch is:

$$E = \widetilde{\rho} \times dE_{ion}/dx \times N_e^{bunch} , \tag{22}$$

where $N_e^{bunch} = 2 \cdot 10^{10}$ is the number of beam electrons in one bunch. From Eq. 22 follows that the amount of energy deposited in the target is $4 \cdot 10^{14}$ eV/bunch corresponding to $6.4 \cdot 10^{-5}$ J/bunch. The local temperature rise induced by this energy depends on the beam spot size at the polarimeter position. In the present design of the Beam Delivery System of TESLA a possible position for the Compton and Møller polarimeters is the straight section of the e$^-$ linac, some few hundred meters before the IP just outside the quads [22]. Within this straight section it is advantageous to place the Møller polarimeter in the region where the beam profile is most spread out having the dimensions of about: $\sigma_x = 75 \mu m$ and $\sigma_y = 7.5\ \mu m$. For the heating calculations we then take the beam spot to be $\Delta x = 4 \times \sigma_x$ and $\Delta y = 4 \times \sigma_y$. The instantaneous temperature rise ΔT, of the target area hit by one beam bunch over that of the liquid nitrogen, is shown in Table 2. The ΔT values given in this Table are thus calculated for a pure iron target of 10 μm thickness taking the beam spot area to be $\Delta x \times \Delta y$ using several σ_x and σ_y values. As can be seen, for the case of $\sigma_x = 75\ \mu m$ and $\sigma_y = 7.5\ \mu m$ one has ΔT = 200 K.

From the values given in Table 2 it is obvious that the local temperature will be above the melting point (1808 K for Fe) if all the bunches within one pulse will hit the same small region of the target foil. To avoid this situation one needs to spread out over the target the individual hitting positions of the train of bunches. A possible solution to this problem is outlined in the next subsection.

4.4.2 The target cooling

In the present design of the next generation of Linear Colliders with large beam currents of 30 - 45 μA and high luminosity values the typical beam sizes are few tens of microns. Therefore in the cases where the beam polarisation measurements utilise a Møller polarimeter, the local target heating requires a special care.

A possible solution to this local heating problem can be the implementation of a rotating disk target cooled down, all around its circumference, to about 110 K by liquid nitrogen. Such a solution for the heating problem has in fact been applied to a Møller polarimeter [23] which operated in an electron beam of 0.8 to 5.0 GeV with a current of 0.5 to 5.0 μA where the needed polarisation measurement time was about 20 min. The envisaged target is placed in such a way that its rotation axis is parallel displaced to the beam direction so that successive bunches hit different regions of the target and they will be distributed over a circle. If the disk rotates with a frequency of about 1000 Hz, around an axis displaced by 2.7 cm from the beam direction, all the impact points of the 2820 bunches of a single pulse, will be spaced by about 60 μm over an annular zone having a width of 300 μm.

Inasmuch that one can neglect the influence of one heated point on the others we evaluate, using the well known heat conduction formulae [24], that each heated spot will be cooled down to ΔT = 0.1 K above the liquid nitrogen temperature within about 2 msec. This short time is mainly determined by the shortest distance to the cooled edge of the target. The residual heating of about 0.5 K/sec results in a final temperature rise of 50 K at the end of a 80 sec operation time needed for a polarisation measurement with a precision of about 1-2 % . Finally the fact that the pause between pulses is even 199 msec one has a sufficient safety margin to cover possible additional minor factors which may affect the cooling time calculations.

The local rise in temperature of about 200 K, causes a relatively negligible target depolarisation since the working point at $\sim$ 110 K lies in the plateau region of the magnetisation curve shown in Fig. 9.

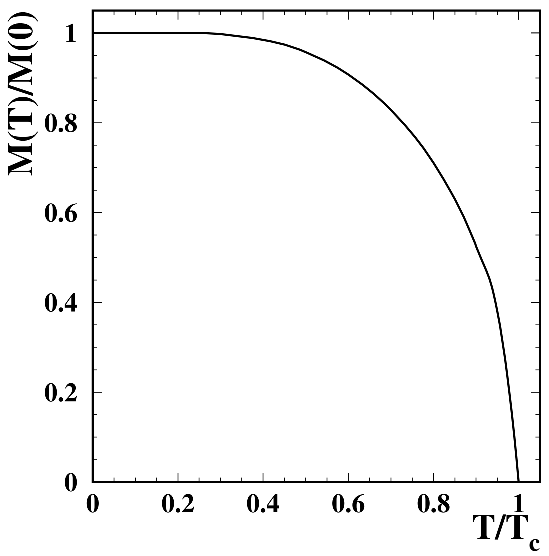

Figure 9: Saturation magnetisation of Fe as a function of the temperature scaled by the Curie temperature $T_c = 1043$ K.

This curve is derived from equation (see e.g. [25])

$$M(T) \;=\; M(0)\tanh\left(\frac{M(T)}{M(0)} \times \frac{T_c}{T}\right), \tag{23}$$

which describes the magnetisation M of the material as a function of T/T_c where T_c is the Curie temperature, e.g. 1043 K for Fe target. For temperatures above T_c the spontaneous magnetisation vanishes. As seen from Fig. 9 at room temperature ($\simeq$ 300 K) or less, the magnetisation depends weakly on T. Assuming the cooling temperature of the target to be 110 K, the increase ΔT of the local temperature given in Table 2 corresponds to a change in the magnetisation of $\Delta M = 0.3$ % for a beam profile of $\sigma_x\sigma_y = 75 \times 7.5$ (μm)^2. Thus the heating of the target does not damage its magnetisation and the corresponding polarisation characteristics.

5 Measurement of the beam polarisation

For the measurement of the electron beam polarisation we consider here a single-arm polarimeter, with a well defined angular and momentum acceptance, including a pixel detector for the Møller scattered electrons. The detector is placed

some 20 meters away from the polarised iron target. Its typical dimension should cover, with a sufficient a large margin, the angular acceptance of the polarimeter which we chose in this work to have the polar angle range of 1.4 to 2.9 mrad. Thus the typical dimension will be of the order of 3.3 cm or its area about 10 cm^2. This area is assumed to be covered in the front by about 10^6 pixels, each having an area $20\mu m \times 50\mu m$.
The electron beam longitudinal polarisation level P_L^B is extracted from the measured A_R asymmetry defined in Eq. 4, which is calculated from the results of the two measured rates obtained from the Møller scattering with two different relative orientations of the beam polarisation vector with respect to that of the target.

The numbers of elastic Møller scattering events are counted for two different relative beam-target polarisation vectors, namely $(\vec{P}^B, \vec{P}^T)$ and $(-\vec{P}^B, \vec{P}^T)$. The number of Møller events integrated over the range x_{min} to x_{max} where x is defined as:

$$x = 2p_{lab}/E_B$$

and summed over the measurement time T_+ and T_- are given by:

$$\begin{aligned} N_+ &= \mathcal{L}_+ T_+ \int_{x_{min}}^{x_{max}} \varepsilon_+(x) \frac{d\sigma}{dx}(1 - P_L^B P_L^T A_L(x))dx\,, \qquad (24) \\ N_- &= \mathcal{L}_- T_- \int_{x_{min}}^{x_{max}} \varepsilon_-(x) \frac{d\sigma}{dx}(1 + P_L^B P_L^T A_L(x))dx\,, \qquad (25) \end{aligned}$$

where $\varepsilon_+(x)$ and $\varepsilon_-(x)$ describe the efficiencies of the polarimeter as a function of x and $\mathcal{L}_+$ and $\mathcal{L}_-$ are the luminosity values for the parallel and anti-parallel beam-target spin states. The functions $d\sigma/dx$ and $A_L(x)$ are the unpolarised Møller cross section and the asymmetry. These are given by the expressions:

$$\begin{aligned} \frac{d\sigma}{dx} &= \frac{2\pi\alpha^2}{s}\frac{[3+(x-1)^2]^2}{[1-(x-1)^2]^2}\,, \\ A_L(x) &= \frac{[7+(x-1)^2][1-(x-1)^2]}{[3+(x-1)^2]^2}\,. \qquad (26) \end{aligned}$$

Eqs. 26 are derived from Eqs. 1, 3 and the relation 12 after integration over the whole azimuthal angle range.

To evaluate the polarimeter performance we choose our optimal measurement domain to be the one shown by the stripped area in Fig. 8 which confines the x range to the limits $x_{min} = 0.66$ and $x_{max} = 1.34$. For simplicity we consider the case where the integrated luminosities and efficiencies for the parallel and anti-parallel polarisations of the beam and target electrons are the same i.e., $\mathcal{L}_+T_+ = \mathcal{L}_-T_-$ and $\varepsilon_+(x) = \varepsilon_-(x) = \varepsilon(x)$. The experimental measured asymmetry A_{exp} is written as:

$$A_{exp} = \frac{N_+ - N_-}{N_+ + N_-} = P_L^B P_L^T < A_L > \ , \tag{27}$$

where the mean value $< A_L >$ is given by:

$$< A_L >= \frac{\int \varepsilon(x)\frac{d\sigma}{dx}A_L(x)dx}{\int \varepsilon(x)\frac{d\sigma}{dx}dx} \ . \tag{28}$$

Thus the beam polarisation,

$$P_L^B = \frac{A_{exp}}{P_L^T < A_L >} \tag{29}$$

is proportional to the inverse of the mean longitudinal asymmetry. The relative error of the measured beam polarisation P_L^B is evaluated from Eq. 29 to be:

$$\left(\frac{\Delta P_L^B}{P_L^B}\right)^2 = \left(\frac{\Delta A_{exp}}{A_{exp}}\right)^2 + \left(\frac{\Delta P_L^T}{P_L^T}\right)^2 \ , \tag{30}$$

where the statistical error on the measured asymmetry is :

$$\Delta A_{exp}^2 = 4\frac{N_+N_-}{N^3} = \frac{1 - A_{exp}^2}{N} = \frac{1}{\mathcal{L}T\sigma_t}\left(1 - (P_L^B P_L^T < A_L >)^2\right) \ . \tag{31}$$

Here N is the total scattering events number recorded within the domain $x_{min} - x_{max}$ i.e.,

$$N = N_+ + N_- = \mathcal{L} \cdot T \cdot \sigma_t \ ,$$

with

$$\sigma_t = \int_{x_{min}}^{x_{max}} \varepsilon(x)\frac{d\sigma}{dx}dx \ \cdot$$

By using Eqs. 31 and 29 we can rewrite Eq. 30 as follows:

$$\left(\frac{\Delta P_L^B}{P_L^B}\right)^2 = \frac{1}{\mathcal{L}T\sigma_t}\frac{1 - (P_L^B P_L^T < A_L >)^2}{(P_L^B P_L^T < A_L >)^2} + \left(\frac{\Delta P_L^T}{P_L^T}\right)^2 \ . \tag{32}$$

Since $(P_L^B P_L^T < A_L >)^2 \ \leq \ 2.4 \cdot 10^{-3}$ (see Table 4), it is negligible in comparison to 1, so that one can simplify Eq. 32 to:

$$\left(\frac{\Delta P_L^B}{P_L^B}\right)^2 \simeq \frac{1}{\mathcal{L}T\sigma_t}\frac{1}{(P_L^B P_L^T < A_L >)^2} + \left(\frac{\Delta P_L^T}{P_L^T}\right)^2 . \tag{33}$$

Thus the time t_{Int} needed to reach a desired relative polarisation precision $\Delta P_L^B / P_L^B$ is given by:

$$\frac{1}{t_{Int}} \simeq \mathcal{L} \left[\left(\frac{\Delta P_L^B}{P_L^B} \right)^2 - \left(\frac{\Delta P_L^T}{P_L^T} \right)^2 \right] \left(P_L^B P_L^T \right)^2 \sigma_t < A_L >^2, \tag{34}$$

which corresponds to the number of scattering events

$$N_{Int} = \mathcal{L} \times t_{Int} \times \sigma_t \tag{35}$$

needed to perform the polarisation measurement. In Table 3 we present the unpolarised cross section and the averaged asymmetry values for several $x_{min} - x_{max}$ regions around $\theta = 90^o$ which may be of interest in a Møller polarimeter design. In Table 4 we list some of the values concerning the characteristics and performance of the proposed TESLA Møller polarimeter. Using Eqs. 27 and 31 and the values listed in columns 1 to 3 of Table 4, we calculated the number of events needed to obtain a relative statistic error of 0.5% for the measured asymmetry A_{exp}. The systematic error associated to the asymmetry A_{exp} measurement comprises the uncertainties coming from : the bremsstrahlung background estimation (1.0 - 1.25 %), the Levchuk effect (0.4 %) and other sources (0.17 %). The relative error of the target polarisation measurement is taken to be 0.5 %. From the previous listed errors we thus obtain for the beam polarisation measurement a relative systematic error up to 1.2 - 1.4 %. Finally we estimate the over-all relative error on the beam polarization measurement to be 1.3 - 1.5 %.
The precision expected from the TESLA polarimeter in a measurement duration of 80 sec is compared in Table 5 with three existing Møller polarimeters in use at high energy electron colliders.

6 Background considerations

The background sources to the Møller scattering signal depend intrinsically on the mode of operation. Whereas in the double-arm polarimeter the bremsstrahlung background is suppressed, its statistics is considerably reduced and it is more sensitive to radiation corrections. In the framework of a one-arm Møller polarimeter applied to the TESLA collider parameters, we consider three possible contributions which might affect the precision of the polarisation measurement.

Multi-hit Møller scattering events

Using the planned electron beam structure of TESLA as given in Table 1, about 16 electrons emerging from the Møller scattering process are expected to reach the polarimeter detector within a time interval of $\sim$1 ps (one bunch lenght) which is followed by a pause of 337 nsec. This means that for a detector of about 10^6 pixels the probability that at least 2 out of the 16 electrons will hit the same pixel is about 2×10^{-4}. The fact that a pixel can record, until it is read out, just one hit means that in the scheme where the detector is read out only after the end of a TESLA pulse, of about 1 msec, a very large part of the Møller scattering events remains unrecorded. This calls for a more frequent read out which, in current available technology, can be achieved within $500 - 1000$ nsec. To overcome the event loss one can adopt e.g. a data taking scheme whereby the detector is read out after $\sim$ 25 bunches. This implies the loss of about $100 - 150$ bunches from the total of 14,100 bunches produced during one second which results in a negligible reduction in the statistics. At the same time the loss due to multi-hit events is substantially reduced to the level of a few percents which can be well accounted for by an a appropriate Monte Carlo simulation study so that its residual contribution to the systematic error of the polarisation measurement is well below 1%.

Deep inelastic scattering (DIS)

In order to estimate the rate of electrons hitting the Møller detector which originated from deep inelastic e^- - Fe nucleus scattering, we apply the Equivalent Photon Expression (EPE) which states that $\sigma^{ep} = f_\gamma \times \sigma^{\gamma p}$. Here σ^{ep} is the total electron-proton cross section, $\sigma^{\gamma p}$ is the total γp cross section and f_γ, the photon flux, is given by:

$$f_\gamma = \int_{y_2}^{y_1} dy \left[\frac{1 + (1-y)^2}{y} \ln \frac{Q^2_{max}}{Q^2_{min}} - \frac{2(1-y)}{y} \left(1 - \frac{Q^2_{min}}{Q^2_{max}} \right) \right] .$$

The parameter $y = 1 - E'/E_B$ and Q^2 are respectively the fraction of the beam electron energy and the four momentum squared transmitted to the target nucleon. Choosing the interval $0.45 < y < 0.55$ that corresponds to the region where the scattered electron is around half of beam energy, as in the Møller process, we calculate the total cross section to be $\sigma^{ep} = 0.7\ \mu b$ leading to a DIS cross section for the Fe nucleus of $\sigma^{eFe} = A_{Fe}^{2/3} \times \sigma^{ep}$. However unlike the Møller differential scattering angles which lies in the 1 to 3 mrad, the DIS angular distribution for the chosen y region is very much peaked in the forward direction namely around the value of $\sim 10\ \mu rad$. Thus the number of the DIS electrons which will pass the angular acceptance of the detector is negligible.

Bremsstrahlung

As is well known the total electron-nucleus bremsstrahlung cross section is independent of the electron energy. It's angular distribution is sharply forward peaked with an average polar angle of $\langle\theta\rangle \sim m_e/E_B$. To estimate the bremsstrahlung background under the Møller scattering signal within the angular and momentum acceptance of the polarimeter we used the expression as given e.g. in Ref. [26]. This general expression was integrated over our polarimeter momentum and angular acceptances. As a result we estimate that the bremsstrahlung process is of the order of 25% of the Møller scattering rate, thus being by far the dominant background source.

Fortunately the bremsstrahlung process is very well modeled in Monte Carlo programs. These programs currently in use by experiments at high energy colliders [6], are known to a precision of $\sim 1.0\%$. In addition this background may also be measured, for example, by placing the Møller polarimeter (its iron foil and pixel detector) once in an electron and once in a positron test beams. Whereas in a given angle the bremsstrahlung contribution to the scattering process is in both cases the same, the Møller cross section of the positrons is only a quarter of that of the electrons. This allows an extraction of the bremsstrahlung contribution to the scattering process which can then serve to check and further tune up the Monte Carlo programs. The angular distribution inferred from the pixel detector can also be used to check the background estimation. Assuming that the simulation leads to an error on the estimation of the bremsstrahlung background at the level of about 5%, already previously reached [20], we calculate its contribution to the systematic error of the polarisation measurements.

Thus it is to be expected that the bremsstrahlung background uncertainty contribution to the polarisation systematic error can be kept down to the level of about 1.0 - 1.25%. This will result in an over-all relative precision of the beam polarisation measurement of not more than $1.3 - 1.5\%$ at the statistic level acquired in 80 sec shown in Table 5. This error will decrease to 1.2 % for an unlimited time measurement.

7 Acknowledgements

We would like to acknowledge the help and support of many members of the TESLA collaboration, in particular our thanks are due to T. Behnke, K. Mönig and P. Schüler. Our thanks are also due to G. Bella and E. Naftali for helping us in the estimation of the background sources to the Møller scattering measurements. One of us (G.A.) would like to thank Profs. T. Hebbeker, T. Lohse and P. Söding for their very kind hospitality during his stay at the Physics Institute of the Humboldt University, Berlin and at DESY/Zeuthen. Finally this work would not have been possible without the generous financial support extended to him by the DFG during his stay in Berlin.

References

[1] F. Zimmermann, *Tutorial on Linear Colliders*, CERN-SL-2000-069 (AP).

[2] *TESLA, Technical Design Report*, Vol I - VI, DESY 2001-011, ECFA 2001-05.

[3] See e.g., G.J. Gounaris, C.G. Papadopoulos, Eur. Phys J. C2 (1998) 365;
A.A. Babich et al., Phys. Lett. B481 (2000) 263;
M. Woods, *Polarimetry at a future linear collider - how precise?*, SLAC-PUB-8397, hep-ex/0004004;
G. Moortgat-Pick, H. Steiner, *Physics Opportunities with Polarized e^- and e^+ Beams at TESLA*, Eur. Phys. J direct C6 (2001) 1-27.

[4] H. Olsen, *Applications of Quantum Electrodynamics*, Springer Tracks in Modern Physics Vol. 44 (1968).

[5] M. Swartz, *Polarization at LEP*, Eds. G. Alexander et al., CERN 88-06, (1988) Vol. 2, p. 163.

[6] M. Swartz et al., Nucl. Inst. and Meth. A363 (1995) 526.

[7] P. Steiner et al., Nucl. Inst. and Meth. A419 (1998) 105.

[8] M. Hauger et al., Nucl. Inst. and Meth. A462 (2001) 382.

[9] J. Arrington et al., Nucl. Inst. and Meth. A311 (1992) 39.

[10] H.R. Band et al., Nucl. Inst. and Meth. A400 (1997) 24.

[11] Spin Muon Collab., Nucl. Inst. and Meth. A443 (2000) 1.
E. Burtin, Ph.D. Thesis, University Paris XI, Orsay, (1996).

[12] L.L. DeRaad Jr. and Y.J. Ng, Phys. Rev. D11 (1975) 1586.

[13] N.M. Shumeiko and J.G. Suarez, Fizica B8 (1999) 97;
N.M. Shumeiko and J.G. Suarez, J. Phys. G26 (2000) 113.

[14] S. Jadach and B.F.L. Ward, Phys. Rev. D54 (1996) 743.

[15] L.G. Levchuk, Nucl. Inst. and Meth. A345 (1994) 496.

[16] A. Afanasev and A. Glamazdin, *Atomic electron motion for Møller polarimetry in a double-arm mode*, hep-ex/9602002.

[17] *Polarised Protons at high Energies Accelerator Challenges and Physics Opportunities,* Eds. A. de Roeck, D. Barber and G. Rädel DESY-PROC-99-03.

[18] M. Battaglia et at., *A Pixel Vertex Tracker for TESLA Detector*, LC-DET-2001-042, hep-ex/0102046.

[19] O. Napoly, *TESLA Linear Collider: Status Report*, to be published in the Proc. of the 5th Linear Collider Workshop 2000, Fermilab, Illinois, USA.

[20] L.V. de Bever et al., Nucl. Inst. and Meth. A400 (1997) 379.

[21] Particle Data Group, Eur. Phys. J. C15 (2000) 164.

[22] K.P. Schüler, *Polarimeter studies for TESLA* , LC-DET-2001-047.

[23] A.V. Glamazdin et al., Fizica B8 (1999) 91.

[24] See e.g., H. Stöcker, *Taschenbuch der Physik*, (Harri Deutsch-Verlag, 1998), Section 22.10 ;
U. Grigull and H. Sandner, *Heat Conduction*, (Springer-Verlag, 1984).

[25] C. Kittel, *Introduction to solid state physics*, (John Wiley & Sons, 1986).

[26] W. Heitler, *Quantum Theory of Radiation*, 3rd Edition (Oxford 1954), p. 244;
See also, H.W. Koch, J.W. Motz, Rev. Mod. Phys. 31 (1959) 920.

List of Tables

Beam Energy	[GeV]	250.0
$\gamma = E_B/m_e c^2$		4.89×10^5
Horizontal normalized emittance	[μm]	10.0
Vertical normalized emittance	[μm]	0.03
Bunch length at IP	[mm]	0.3
Bunch population		2.0×10^{10}
Number of bunches		2820
Bunch separation	[ns]	337
Repetition Rate	[Hz]	5.0
Averaged current	[μA]	45

Table 1: TESLA beam characteristics.

$\Delta x \Delta y$ $[\mu m]^2$	400×40	320×30	300×30	240×30
ΔT [^{o}C]	113	188	200	250

Table 2: The instantaneous local temperature rise, ΔT [^{o}C], of the target within the beam spot $\Delta x \Delta y$ during one bunch of ~ 1 ps before the heat is spread over the target.

θ_{CM} [degree]	90 ± 10	**90 ± 20**	90 ± 30	90 ± 40	90 ± 50
θ_{lab} [mrad]	1.70 – 2.41	**1.42 – 2.89**	1.17 – 3.50	0.94 – 4.33	0.74 – 5.56
$x_{max} - x_{min}$	1.17 – 0.83	**1.34 – 0.66**	1.5 – 0.5	1.64 – 0.36	1.76 – 0.26
$\sigma_t/(2\pi\alpha^2/s)$	3.336	**6.831**	11.667	18.624	32.404
$< A_L >$	0.765	**0.730**	0.668	0.583	0.459
$< A_L^2 >$	0.585	**0.534**	0.453	0.357	0.242
$\frac{<A_L^2>-<A_L>^2}{<A_L^2>}$	0.1%	**0.3%**	2%	5%	13%

Table 3: The characteristic unpolarised cross sections and average asymmetries for Møller scattering calculated for $E_B = 250$ GeV. The boldfaced values represent the optimal working range marked in Fig. 8.

$P_L^B \cdot P_L^T$	σ [$\mu barn$]	$< A_R >$	t_{Int} [sec]	N_{events}
$0.8 \cdot 0.5$	0.274	0.292	2	$4 \cdot 10^5$
$0.8 \cdot 0.2$	0.342	0.117	12	$3 \cdot 10^6$
$0.8 \cdot 0.1$	0.364	0.058	53	$12 \cdot 10^6$
$0.8 \cdot 0.08$	0.369	0.047	79	$18 \cdot 10^6$

Table 4: The features of a 100% efficient Møller polarimeter, operating at a relative statistical error of 0.5 %, within an x acceptance between 0.66 to 1.34 and an azimuthal range of $\Delta\phi = 40^o$. The values given are for a 250 GeV electron beam.

	JLAB [8]	**E154 @ SLC [10]**	**SLD @ SLC [6]**	**TESLA**
Target	Fe	Fe+Co Alloy	Fe+Co Alloy	Fe
E_B [GeV]	1 – 6	48	46.6	250
θ_{lab} [mrad]	32 – 13	4 & 9	4.5	2.0
p_{lab} [GeV]	0.5 – 3	24	23.3	125.0
$(\Delta P_L^B/P_L^B)_{syst}$	0.5 %	2.7 %	4.2 %	$\simeq$ 1.3%
$\Delta P_L^B/P_L^B$	$\simeq$ 1.1 %	$\simeq$ 2.7 %	$\simeq$ 4.4 %	$\simeq$ 1.4%

Table 5: A comparison of several representative parameters of three existing Møller polarimeters with the proposed configuration for TESLA. The θ_{lab} and p_{lab} values are calculated for the CM angle $\theta = 90^o$. The over-all precision of the beam polarisation measurements, $\Delta P_L^B/P_L^B$, is also listed. The quoted $\Delta P_L^B/P_L^B$ value given for TESLA corresponds to a measurement duration of 80 sec (see Table 4).